IEEE Access
Multidisciplinary | Rapid Review | Open Access Journal

Received May 5, 2022, accepted June 10, 2022, date of publication June 16, 2022, date of current version June 23, 2022.

Digital Object Identifier 10.1109/ACCESS.2022.3183800

Miniaturized Multiband Metamaterial Antennas With Dual-Band Isolation Enhancement

CHRISTOS MILIAS[1,2], (Student Member, IEEE), RASMUS B. ANDERSEN[1], PAVLOS I. LAZARIDIS[3], (Senior Member, IEEE), ZAHARIAS D. ZAHARIS[4], (Senior Member, IEEE), BILAL MUHAMMAD[2], JES T. B. KRISTENSEN[1], ALBENA MIHOVSKA[2], (Member, IEEE), AND DAN D. S. HERMANSEN[1]

[1]MyDefence ApS, 9400 Nørressundby, Denmark
[2]Department of Business Development and Technology (BTECH), Aarhus University, 7400 Herning, Denmark
[3]School of Computing and Engineering, University of Huddersfield, Huddersfield HD1 3DH, U.K.
[4]Department of Electrical and Computer Engineering, Aristotle University of Thessaloniki, 54124 Thessaloniki, Greece

Corresponding author: Christos Milias (cm@mydefence.dk)

This work was supported by the Project MObility and Training fOR beyond 5G ecosystems (MOTOR5G) through the European Union's Horizon 2020 Programme of the Marie Skłodowska-Curie Actions (MSCA) Innovative Training Network (ITN) under Grant 861219.

ABSTRACT We present electrically small, multi-band, metamaterial-inspired antennas with adequate radiation characteristics and isolation enhancement. The antenna element consists of a complementary split-ring resonator (CSRR) embedded in a small monopole that has a size of $\lambda/8 \times \lambda/10$ at the lowest frequency band, while rectangular patches are placed underneath it to further improve the performance. The antenna operates at the 2.4-2.5/2.9-4.8/5.1-6.5 GHz frequency bands. Moreover, we propose a systematic, metamaterial-based approach in order to improve the isolation between two of these small, closely spaced antenna elements at the lowest and highest frequency bands. The proposed techniques reduce the coupling by up to 29 dB without increasing the size of the structure. In particular, the isolation enhancement at the highest frequency band of interest is remarkably wideband. The cable effect, which is a common concern during the measurements of small antennas, is examined as well. The proposed antennas are not only small but also densely packed and can be easily integrated with modern, compact communication devices with advanced functionality. Simulations along with experimental results validate the effectiveness of our design.

INDEX TERMS Isolation enhancement, metamaterials, multi-band antennas, small antennas.

I. INTRODUCTION

Electrically small antennas (ESAs) have drawn broad interest due to their small footprint that makes them attractive for various applications. The necessity for compact and functional transceivers requires new antenna designs, where the elements shall not only be efficient and multi-band but also small and low-profile. Unfortunately, ESAs suffer from narrow bandwidth and low efficiency as they have fundamental limitations that have been explored by many authors [1]–[4]. In an effort to overcome these limitations metamaterials have gained focus. Metamaterials are man-made structures that have exotic electromagnetic properties such as the realization of negative permittivity and permeability. Due to their unique characteristics, metamaterials are widely used for antenna miniaturization, isolation enhancement and many other antenna and microwave applications [5]–[17]. A sub-wavelength dipole surrounded by a metaresonator is examined in [18], where the metaresonator compensates for the capacitive nature of the short electric dipole and improves the impedance matching. Some variations of electrically small monopoles are proposed in [19] and [20]. The small monopoles are placed in proximity to a split-ring resonator (SRR) and electric-LC (ELC) resonator respectively, thus resulting in compact size. A compact tri-band monopole with single-cell metamaterial loading and defected ground structure is proposed in [22]. It should be stressed that metaresonator-based antennas do not strictly utilize the metamaterial properties of negative permittivity or permeability but mostly rely on the metaresonator (e.g. SRR, ELC) and radiator (antenna element) interaction to achieve miniaturization. This approach is reasonable, since in order to macroscopically synthesize an effective metamaterial medium, a periodic arrangement of several unit cells is necessary.

The associate editor coordinating the review of this manuscript and approving it for publication was Yang Yang.

Hence, there would be an immediate size increment, which is opposed to the goal of these designs.

Furthermore, modern communication devices shall include many antennas in order to fulfill the demanding specifications. The main challenge of multi-antenna systems such as MIMO and phased arrays is the inter-element coupling, which is detrimental to their performance. MIMO systems typically require at least -17 dB levels of isolation for adequate envelope correlation coefficient and error rate [23]–[25]. Phased arrays have more strict coupling requirements in order for the active VSWR to be kept low as the scan angle varies and for maintaining high amplifier efficiency [26], [27].

Metamaterials (MTMs) are also widely utilized for antenna decoupling. In particular, Single-Negative (SNG) metamaterials that possess either negative permittivity (Epsilon-Negative, $\epsilon < 0$) or negative permeability (Mu-Negative, $\mu < 0$) prohibit the propagation of electromagnetic waves since the propagation constant becomes real, i.e, $\gamma \in \mathbb{R}$ [28]. The waves inside this artificial medium are evanescent. This feature is attractive for minimizing the cross-talk and enhancing the isolation between adjacent antennas. A method for the decoupling of two closely spaced monopoles is proposed in [29], where a metamaterial cell is inserted between the antennas. Two meander-like structures are placed between two patch antennas in [30] and an isolation improvement of 16 dB is reported. An isolation technique based on SNG MTMs for densely packed monopoles is proposed in [31]. This metamaterial structure acts as a filter that exhibits a stop-band response at the frequency interval of interest. In a similar way, SRR inclusion pairs are inserted between monopoles in [32] and result in 25 dB coupling reduction. The downside of the aforementioned studies is that the isolation is enhanced only within a narrow window of operation or at a single frequency due to the narrow-band nature of these metaresonators.

Regarding dual-band isolation improvement, the authors of [33] present a methodical approach for the design of a metasurface that considerably decreases the coupling between two adjacent elements at two distinct frequency bands. Unarguably, the superstrate increases the volume of the platform as well and thus it might be an unsuitable method for several applications with space limitations. Dual-band isolation enhancement is also reported in [34] by utilizing an electromagnetic bandgap (EBG) structure, but the distance between the antennas is somewhat increased since the EBG has a considerable size. In [35], a defected ground structure (DGS) and a meandering branch reduce the coupling at the lower and higher frequency band of two inverted-F antennas respectively. A dual-band 4-antenna MIMO system based on self-decoupled antennas is reported in [36]. Sufficient isolation is achieved by adopting a common grounding branch as the decoupling element. Another dual-band decoupling scheme is studied in [37], where a grounding branch and a T-shaped stub are inserted between two dual-band, closely spaced, 5G monopole antennas in order to create opposite currents which cancel the original coupled ones. Nevertheless, the corresponding bandwidths in which the coupling is reduced are not very wide. A dual-band decoupling network is reported in [38]. Here, the coupling via free space is cancelled by the secondary coupling path via the decoupling circuit at two different frequency bands. Following a similar rationale, a decoupling and matching network (DMN) for single- and dual-band two element antenna arrays is demonstrated in [39]. The network offers significant coupling reduction while simultaneously satisfying the desired impedance matching of the antennas. A novel dual-band DMN is presented in [40]. The DMN consists of a grid of metallic stubs that is inserted between neighboring antenna elements. A procedure is proposed to choose which of the stubs to connect and which not in order to cancel the free space coupling. By utilizing a genetic algorithm to find the required connections, the isolation levels are considerably improved at two distinct frequency bands. Unfortunately, these decoupling networks are complex and bulky. As a result, they are unsuitable for small and low-profile antenna platforms where maintaining a small footprint is crucial. To solve this issue, a compact decoupling network consisting of dummy reactive elements is reported in [41] and dual-band coupling reduction is accomplished without increasing the size of the antenna platform.

In this study, we initially present an electrically small, multi-band, metamaterial antenna, with a size of $\lambda/8 \times \lambda/10$ at the lowest frequency band. The proposed antenna is composed of a monopole loaded with a CSRR, while conducting squares are also placed underneath to further reduce the size of the structure. The unloaded antenna operates from 2.8 to almost 7 GHz, with resonances at 3.2 and 6.5 GHz. A multi-band operation at 2.4-2.5 GHz, 2.9-4.8 GHz and 5.1-6.7 GHz is observed after the metamaterial loading. In particular, the two new resonant modes at 2.4-2.5 GHz and 5-6 GHz bands, which are used for WLAN, are attributed to the presence of the CSRR. Therefore, the first contribution of this paper is the methodical design of an electrically small antenna with multi-band operation and sufficient bandwidth and radiation efficiency within the multiple frequency bands of interest. Compared to previous works, the proposed antenna element features smaller size and improved overall performance. As a next step, we propose SNG metamaterial structures for enhancing the isolation between two of the previously designed, closely spaced ESAs at two distinct frequency bands. The coupling is reduced from -11 dB to -26 dB at 2.45 and from -16 to -45 dB at 5.8 GHz, respectively. Compared to the existing literature, the proposed metamaterial-inspired decoupling scheme occupies less space and is an ideal solution for small antenna platforms where size limitations prohibit the use of other dual-band coupling reduction techniques. Furthermore, it should be pointed out that the isolation improvement at the highest band is remarkably wideband. Both the antenna and decoupling structure design are systematic. The proposed antenna platform is extremely compact, multi-functional

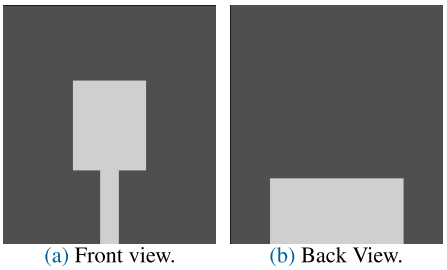

(a) Front view. (b) Back View.

FIGURE 1. Unloaded, printed monopole antenna fed by a microstrip line.

and highlights the benefits of metamaterials in antenna design.

The rest of this paper is organized as follows. In Section II, we present the design of the electrically small antenna. Section III provides the design of metamaterial structures for isolation enhancement. Section IV draws some conclusions.

II. ELECTRICALLY SMALL ANTENNA DESIGN

The design of electrically small antennas faces the challenges of narrow bandwidth and low efficiency. We try to compensate for this by presenting a methodical design of an ESA with sufficient radiation characteristics. The initial, unloaded monopole antenna is illustrated in Fig. 1. It is printed on a low-cost FR-4 substrate with a dielectric constant of $\epsilon_r = 4.3$, loss tangent $tan\delta = 0.025$, substrate thickness $h = 1.6$ mm and copper thickness $t = 0.035$ mm. The monopole is fed by a standard 50 Ω microstrip line.

A. CSRR DESIGN

The CSRR is a metaresonator with subwavelength dimensions, typically $\lambda/10$. It is excited by a time-varying, electric field perpendicular to its axis and is depicted in Fig. 2a. The reason for considering a CSRR cell in this work is twofold: i) it has a small size compared to the wavelength of operation and thus it is suitable for the design of electrically small antennas ii) it exhibits a dual-band response which is exploited in this paper for the design of the small dual-band antenna. The first step of the antenna design is to find the CSRR's proper geometric parameters so that it resonates at the desired bands (WLAN). The most effective way is utilizing electromagnetic simulation tools. The simulation setup of the CSRR is illustrated in Fig. 2b, where Perfect Electric Conductor (PEC) and Perfect Magnetic Conductor (PMC) boundary conditions have been applied. Due to the boundary conditions, the configuration of the setup is equivalent to an infinite periodic arrangement of CSRRs under plane wave illumination with the electric field being normal to the CSRR's surface. Although we are interested in the resonant frequency of a single CSRR unit cell, this configuration can still offer a valuable insight and is considered as a decent approximation. This simulation setup, which is commonly utilized for examining the performance of large metasurfaces, is proven to be an extremely useful tool for finding the parameters of a single CSRR and predicting its electromagnetic response in a quick manner. Moreover, the antenna

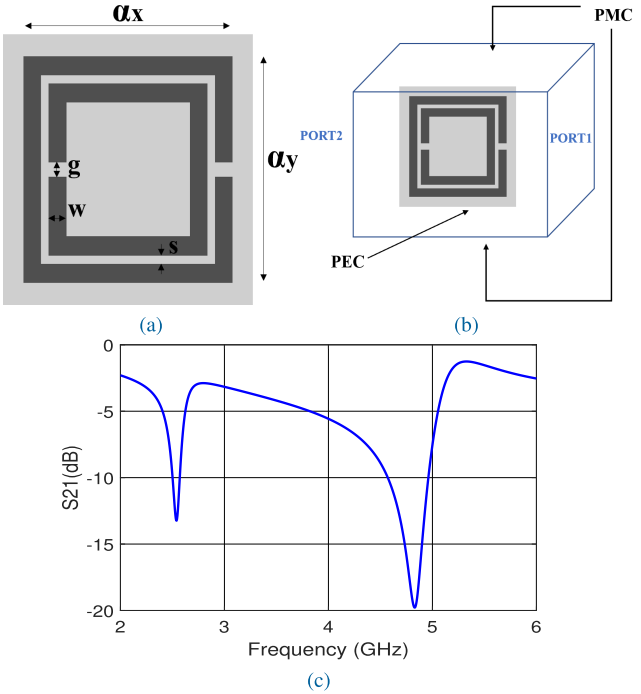

FIGURE 2. (a) The geometry of a CSRR unit cell, (b) its simulation setup and (c) the optimized transmission coefficient S_{21}. Light grey depicts metallization. The CSRR parameters in millimeters are: $\alpha_x = 8.3, \alpha_y = 8.3, w = 0.7, s = 0.3$ and $g = 0.5$.

design is considerably facilitated with prior knowledge of the CSRR's parameters. The most important parameters are its outer dimensions α_x and α_y. Therefore, we choose to keep the values for the other parameters fixed (given the PCB fabrication constraints) and tune α_x and α_y. The transmission coefficient $S21$ of the unit cell is shown in Fig. 2c. After some parametric sweeps, the first resonance is tuned at 2.45 GHz and the second one at 4.9 GHz. The simulations were carried out with the electromagnetic, frequency domain solver of CST Microwave Studio (CST MWS) [43].

B. COMPOSITE ANTENNA

The composite antenna is shown in Fig. 3. The CSRR is not etched exactly at the center of the monopole but at a relative distance of F_x and F_y in x and y axis, respectively. The values of F_x and F_y are chosen carefully so that enough power is being coupled to the metaresonator and ensuring good impedance matching at the same time. Small slots are etched at the intersection of the microstrip line and the monopole (inset feed) to further improve the impedance matching. It is important to note that the previous simulations of the CSRR cell provided an accurate estimation of its geometric parameters. More specifically, both of the CSRR's resonances are slightly shifted towards higher frequencies and the composite antenna resonates around 2.65 GHz and 5.5 GHz after the incorporation of the metaresonator. In order, to further decrease the resonant frequency to 2.45 GHz, we exploit the space underneath the monopole by placing a periodic structure that is composed of rectangular squares. The squares

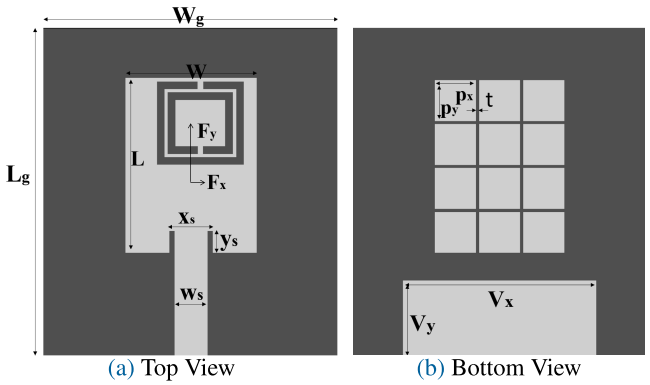

FIGURE 3. The proposed electrically small antenna. The optimized geometric parameters of the antenna in millimeters are: $W = 11$, $L = 15$, $x_s = 4$, $y_s = 2$, $W_g = 27$, $L_g = 30$, $w_s = 3$, $V_x = 18$, $V_y = 7$, $p_x = p_y = 3.7$, $t = 0.3$, $F_x = 0.85$, $F_y = 3.85$, $\alpha_x = 7.8$, $\alpha_y = 8$, $w = 0.7$, $s = 0.3$, $g = 0.3$.

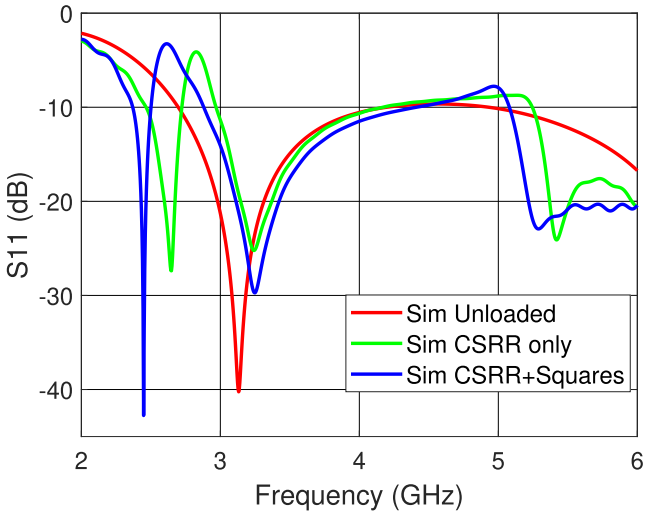

FIGURE 4. Reflection coefficient S_{11} versus frequency derived through simulations of the antenna being unloaded, loaded with CSRR only, and loaded with CSRR and Squares.

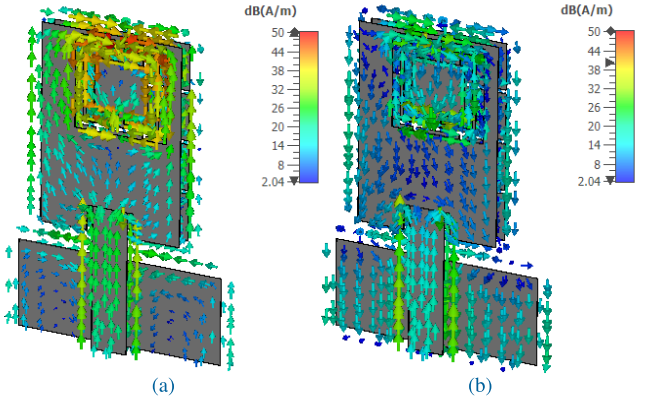

FIGURE 5. Snapshot of the antenna's current distribution at (a) 2.45 GHz and (b) 5.8 GHz.

are equivalent to a reactive loading and as the antenna is in principle an RLC resonator, an additional reduction of the resonant frequency is accomplished. The simulated reflection coefficients of the unloaded, CSRR-only loaded and CSRR+Squares loaded monopoles is depicted in Fig. 4. As illustrated, the loaded antenna exhibits two new resonant frequencies at 2.45 and 5.5 GHz that are not present in the unloaded case. These new resonant modes are clearly attributed to the metaresonator loading, as Fig. 5 verifies, where it is shown that the antenna's surface currents circulate around the CSRR at 2.45 GHz and 5.8 GHz. Despite the fact that the second resonance is centered around 5.5 GHz, the distribution at 5.8 GHz is presented here since it is a commonly used frequency. The dimensions of the rectangular monopole are $\lambda/10 \times \lambda/8$ at 2.45 GHz and therefore is regarded as electrically small. The simulated radiation efficiency is 64% and 80% at the lowest and highest frequency of the design and is adequate given the small dimensions and the lossy FR-4 substrate.

In order to evaluate the performance of the designed ESA, we utilize the quality factor Q. The Q value is given by:

$$Q = \frac{1}{\sqrt{2}\, FBW} \tag{1}$$

where FBW is the fractional -10 dB bandwidth which equal to 130 MHz for the proposed ESA. There is a fundamental limitation between the maximum dimension of an antenna and its minimum Q, commonly referred as Chu limit:

$$Q_{Chu} = \frac{1 + 2(k\alpha)^2}{(k\alpha)^3[1 + (k\alpha)^2]} \tag{2}$$

The Chu limits applies to ideal, lossless antennas and therefore a more suitable criterion is [44]: $Q_{Chu,lossy} = \eta Q_{Chu}$. Here, η is the radiation efficiency. In this manner, the ratio $Q/Q_{Chu,lossy}$ provides a fair evaluation of how well the antenna exploits its volume. The calculated ratio for our antenna is equal to 7.53 and indicates that it has an efficient current distribution.

C. INFLUENCE OF THE CABLE AND GROUND PLANE

Theoretically, a monopole should be placed over an infinite ground plane that provides the necessary image currents for the antenna to operate properly. In practice, this is impossible and the ground plane has finite dimensions. As a result, the attached cable becomes a part of the antenna and the measurements are usually inaccurate and not repeatable. This is a common issue associated with the measurement setup of small antennas and is attributed to two factors: i) common mode currents flowing along the outer conductor of the coaxial cable [45], ii) scattering and secondary radiation caused by the cable. The impact on the impedance and radiation properties can be significant, especially at lower frequencies where the antennas, and consequently their ground planes, are electrically small [46]. Typically, ferrite beads are utilized to deal with this problem during the measurement [47] but they are not an appropriate solution for frequencies higher than 1 GHz as they become extremely lossy. A more suitable approach is the use of a balun that effectively suppresses the cable currents and allows for more accurate measurements

of the antenna under-test (AUT). The drawback of baluns is their narrow-band response that limits their use to a 10% measurement bandwidth.

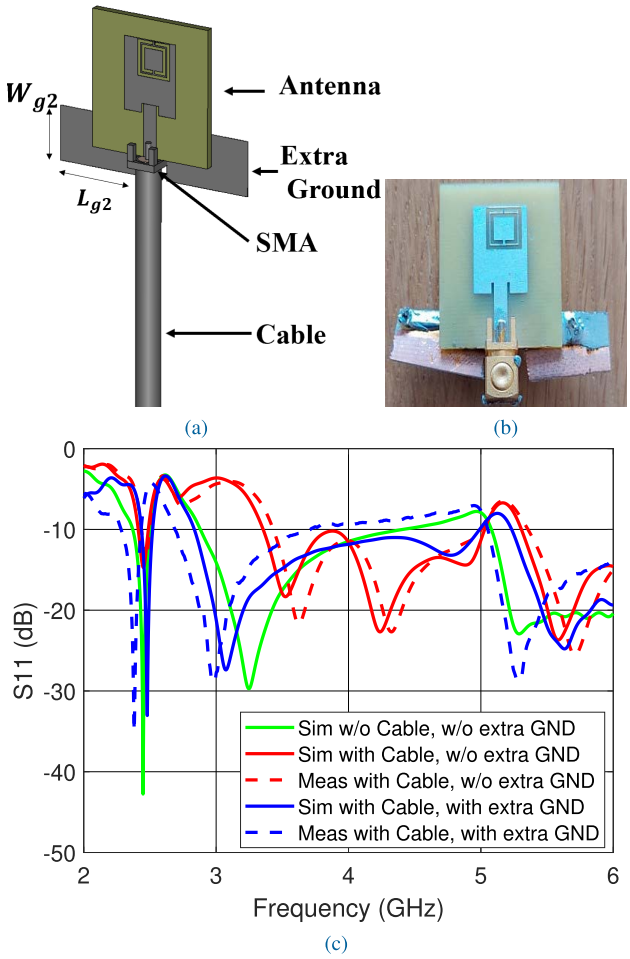

FIGURE 6. (a) Simulation of the antenna with the attached cable and extended ground plane in order to model the measurement setup, (b) fabricated prototype with extra ground plane and connector and (c) simulated and measured reflection coefficient S_{11} versus frequency for different configurations of the antenna. The cable that is considered here has a characteristic impedance of 50 Ω and a length of 150 mm.

In order to solve this issue and to accurately model the measurement setup, we simulated the antenna connected to a coaxial cable as shown in Fig. 6a. As expected, the cable alternates the performance of the antenna. In particular, there is a dramatic change of the input impedance as the length of the cable varies. To prevent this from happening during the measurement, we decided to slightly extend the ground plane of the antennas so that it has a sufficient electrical size. We found the minimum required length and width of the additional ground plane for minimizing the cable effect: $L_{g2} = 1.9\ cm$, $W_{g2} = 1.3\ cm$. This allows for repeatable impedance and radiation pattern measurements, since the antenna becomes immune to variations of the cable length and position. Of course, the size of the antenna is somewhat increased and the results are modified compared to the initial case but this is only required for measurement purposes. Obviously, the influence of the cable cannot be completely suppressed with this method and there are still variations but this is the most convenient way to verify the effectiveness of the design. In particular, the resonant frequencies are not affected at all by the cable after the ground extension. The fabricated antenna with the extended ground plane is depicted in Fig. 6b, while the simulated and measured reflection coefficient with the cable and extra ground are presented in Fig. 6c. As shown, the measured return loss of the antenna with the cable attached to it and without an extended ground plane differs significantly from the initial simulation without the cable. This verifies the dramatic impact of the cable during the measurements. On the other hand, extending the ground plane minimizes this effect and allows for a better characterization of the antenna. A small discrepancy in the resonant frequencies is observed due to an uncertainty of the FR-4's dielectric constant. Therefore, the fabricated antenna resonates at 2.37 GHz instead of 2.45 GHz.

The measured, normalized, H-plane (azimuth) radiation patterns of the antenna with the extra ground at 2.4 GHz and 5.8 GHz are shown in Fig. 7. The measured E-plane (elevation) patterns are provided in Fig. 8. The measurements are compared with the simulated results of the antenna without extra ground. As shown, the antenna has an almost omnidirectional pattern in the azimuth plane at both frequencies. The vertical polarization (Co-pol), where the electric field is parallel to the input microstrip line, is the dominant one. The cross-polarisation levels are at least 15 dB lower compared to the co-polarisation at both bands. Regarding the E-plane (elevation), the radiation patterns are similar to the ones of a typical monopole antenna. The cross-polarisation levels are extremely low (below −20 dB). Furthermore, the 2.4 and 5.8 GHz patterns are quite similar to each other and thus consistent and god performance is expected for a communication system that utilizes both the lower and higher frequency bands of this design. In general, the measured results agree well with the simulations with only minor discrepancies being observed. Hence, the theory and simulation setup are validated successfully. There is a good correlation and the behavior of the antenna is not considerably alternated despite the modification. As anticipated, the antenna has a radiation pattern that resembles the one of a standard quarter-wavelength monopole, while the cross-polarization (horizontal polarization) levels are sufficiently low. All the simulated patterns are normalized with respect to the maximum value of the simulated co-polarisation, while the measured ones are normalized with respect to its measured value.

III. ISOLATION ENHANCEMENT

A. DECOUPLING MEANDERS DESIGN

In order to keep the size of antenna platforms as small as possible so that they fit in compact devices, the elements have to be placed in vicinity. As a result, the coupling between them is of sufficient magnitude and causes performance degradation. To demonstrate this, we consider two

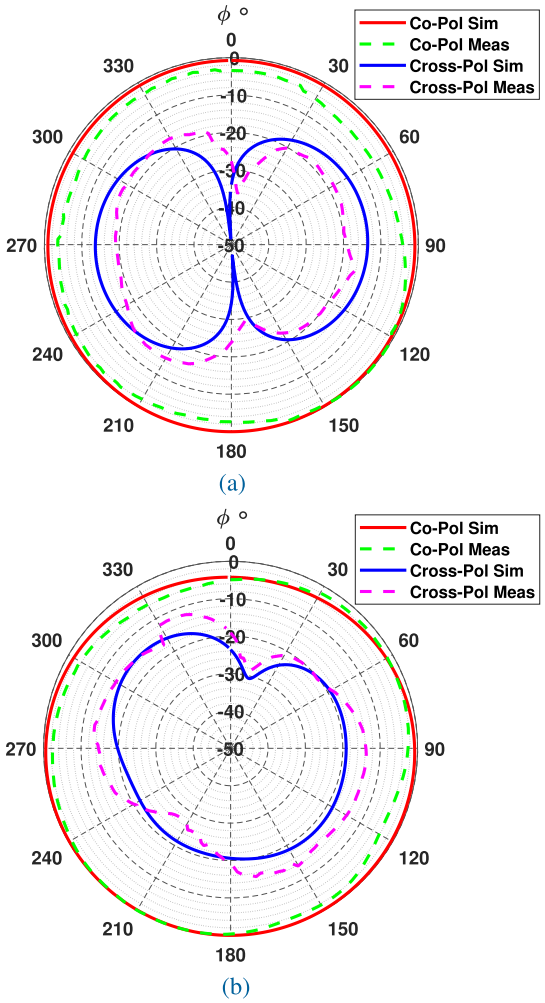

FIGURE 7. Normalized H-plane radiation patterns of the proposed small antenna at (a) 2.4 GHz and (b) 5.8 GHz. The simulations do not include the ground plane extension that was utilized during the measurements.

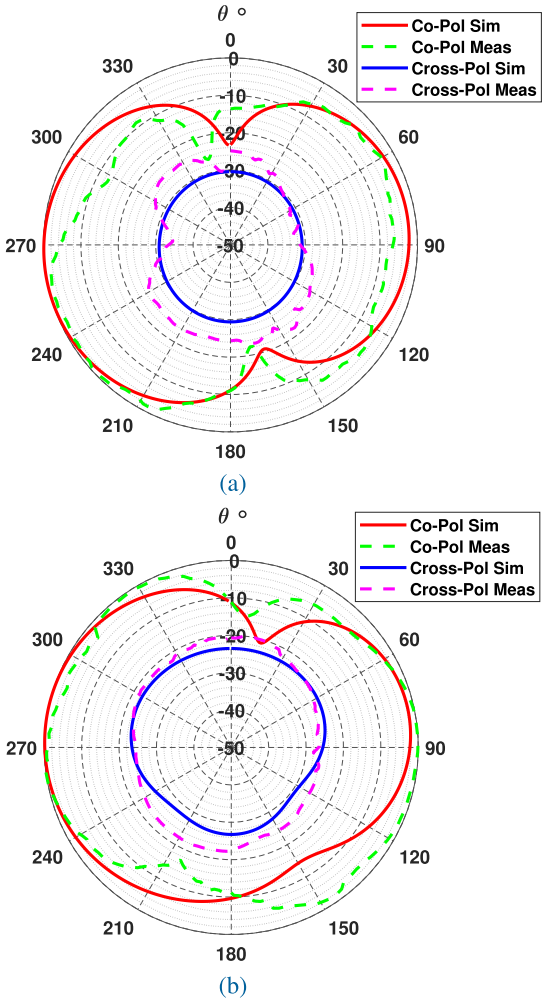

FIGURE 8. Normalized E-plane radiation patterns of the proposed small antenna at (a) 2.4 GHz and (b) 5.8 GHz. The simulations do not include the ground plane extension that was utilized during the measurements.

CSRR loaded monopoles with an edge-to-edge distance of 0.13λ at 2.45 GHz. The coupling between the antennas is expressed by the coefficient $S21$, which has high values varying between −10 and −16 dB across the frequency bands of interest. In this work, only two antennas are considered to demonstrate the decoupling methodology. Nevertheless, the techniques can be extended to antennas with higher number of ports. Meanwhile, 2-port systems are still valuable for small, low-cost platforms such as wearable, mobile, IoT (Internet of Things) and drone communication devices. In order to decrease the coupling, we utilize the meander of Fig. 9a, which has a metamaterial behavior. The meander is excited by a time-varying magnetic field perpendicular to its surface and exhibits negative permeability around its resonant frequency. Moreover, wave propagation is prohibited in metamaterial media with negative permeability since the propagation constant becomes real. By exploiting this property, the coupling can be significantly reduced. In addition, the magnetic field of the monopoles, which is responsible for the coupling, has the proper polarization for the meander's excitation. As we are interested in improving the isolation levels at 2.4 GHz and 5.8 GHz, meanders of different sizes have to be placed, each one corresponding to a specific frequency band.

For the design of the meanders, we follow the same simulation approach as in the case of the CSRR cell. The only difference is that the boundary conditions of the simulation setup are inversed (i.e. replace PEC with PMC and PMC with PEC) in order to excite the meanders with a normal magnetic field. In a similar way to the design of the CSRR, this simulation method facilitates the design process and allows for extraction of the effective permeability. This setup is typically utilized for the design of large-scale metasurfaces and is not completely suitable for examining the performance of few meta-cells. Nevertheless, it is a useful tool for designing metamaterial-inspired structures, finding the appropriate geometric parameters and studying their electromagnetic behavior. This is particularly important for small antenna systems where space limitations prohibit the placement of large metasurfaces with many metamaterial cells. After a parametric sweep, the optimized parameters of the meanders are found and shown in table 1, while their transmission

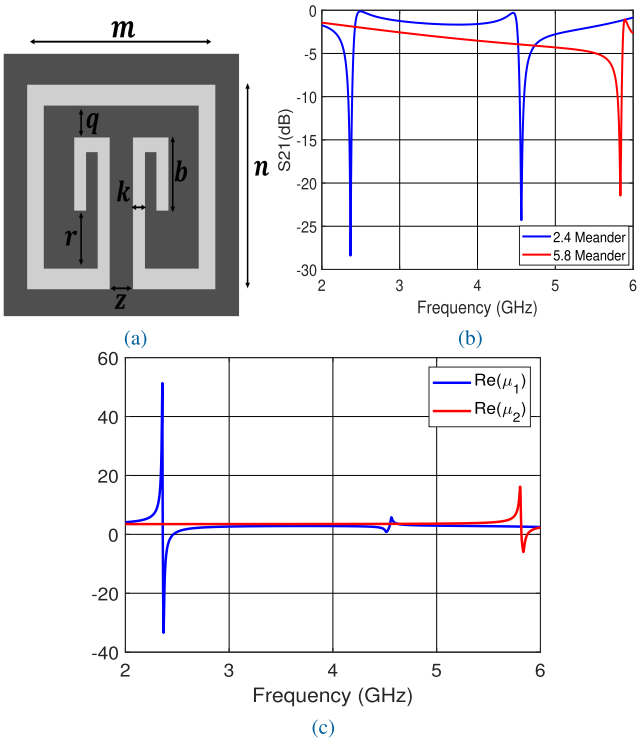

FIGURE 9. The geometry of the meander (a), the optimized transmission coefficient (b) and the extracted effective real permeability of the meander that resonates at 2.4 GHz (index 1) and the meander that resonates at 5.8 GHz (index 2) (c).

coefficient S_{21} is depicted in Fig. 9b. The effective permeability is extracted as well and presented in Fig. 9c, where the following equations are utilized for the extraction [49], [50]:

$$z = \sqrt{\frac{(1+S_{11})^2 - S_{21}^2}{(1-S_{11})^2 - S_{21}^2}} \tag{3}$$

$$e^{jnk_0d} = \frac{S_{21}}{1 - S_{11}\frac{z-1}{z+1}} \tag{4}$$

$$\mu = nz \tag{5}$$

Here, n is the refractive index, z is the impedance, k_0 is the wavenumber of free-space, d is the maximum dimension of the meta-cell, while S_{11} and S_{21} are its reflection and transmission coefficients, respectively. The real permeability of the meanders turns out to be negative at their resonance frequency as anticipated.

B. FINAL ANTENNA PLATFORM

Regarding the integration of the decoupling metamaterials with the antenna platform, the meander resonating at 2.4 GHz has a larger size and the space between the elements allows for the placement of only one. It is stressed again that although a single metamaterial cell does not exhibit negative permeability, quite a similar response is expected. In addition, by taking into account that the antennas have a relatively low efficiency at 2.4 GHz and that the meanders increase the losses due to their small size, placing a lot of them would be detrimental to the radiation characteristics. By observing

TABLE 1. Optimized parameters of meander 1 (2.45 GHz) and meander 2 (5.8 GHz).

Parameter (mm)	Meander 1	Meander 2
m	7.4	6.92
n	7.4	2.8
q	1	0.5
b	4	0.7
r	1	0.3
z	1	1
k	0.5	0.5

the power flow when port 1 (left antenna) is excited and port 2 (right antenna) is matched (connected to 50 Ω load), we can identify the positions where there is a strong field concentration and place the meander at this exact location. Of course, the meander should not be in the vicinity of the microstrip line, since it can act as a stop-band filter and reflect most of the power back to the source, thus leading to poor impedance matching and low total efficiency. By taking the aforementioned into account, we choose the center of the board as an ideal location for the 2.4 meander. Concerning the higher frequency band, the meanders at 5.8 GHz have a smaller size and the antennas have a high radiation efficiency due to their larger electrical length. Hence, many of them can be placed between the elements without distorting their performance. Care must be taken so that the 5.8 meanders do not interact with the 2.4 meander, as this would detune both of them and require further design effort.

The configuration of the adjacent elements with the corresponding decoupling meanders between them is illustrated in Fig. 10a. As depicted, a single 2.4 meander is placed exactly between them at the top layer, while five 5.8 meanders are placed on the top and three more at the bottom layer. The comparison between the simulated coupling coefficient with and without the decoupling unit cells is shown in Fig. 10b. The isolation levels improve from 11 to 26 dB and from 15 to 44 dB at 2.45 and 5.8 GHz, respectively. Despite the fact that the isolation at the lowest frequency is narrowband, it is substantial and covers the corresponding band of 2.4-2.5 GHz. On the other hand, the 5.8 GHz meanders provide a wideband decoupling performance that covers the whole 5-6 GHz frequency window. The superior performance at higher frequencies is attributed to the fact that more meanders were placed between the monopoles, thus resulting in an improved approximation of an SNG metamaterial medium. In addition, it is observed that the metamaterials have minimal effect on the impedance matching and consequently on the reflection coefficients S_{11} and S_{22} of the elements.

To better understand the electrodynamics of the structure, the electromagnetic power flow within the antenna board is depicted in Fig. 11 (the simulator's scale varies from 12.6 to 52.6 VA/m^2 in dB), which provides an insightful illustration of the interaction between the monopoles. Unarguably, the cross-talk is reduced after the introduction of the

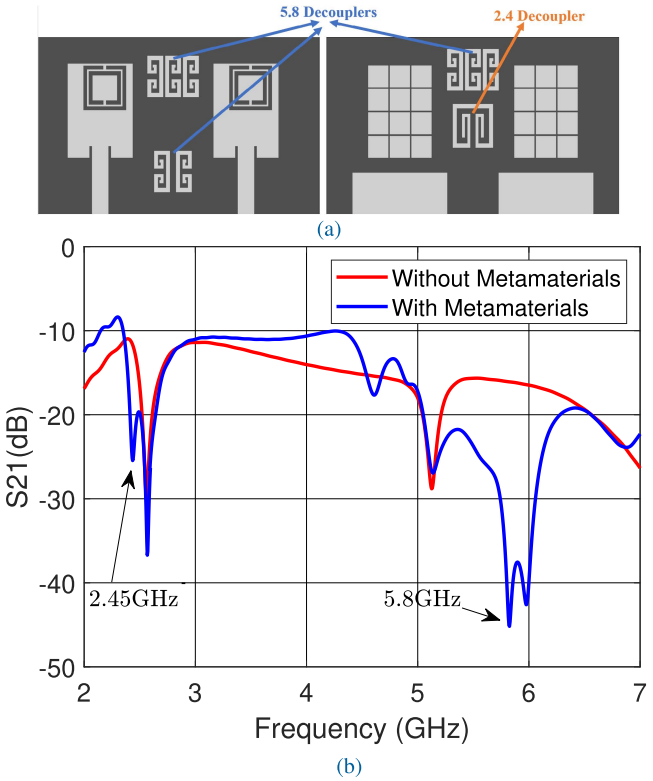

FIGURE 10. (a) Antennas using decoupling structure and (b) coupling coefficient S_{21} derived through simulations versus frequency.

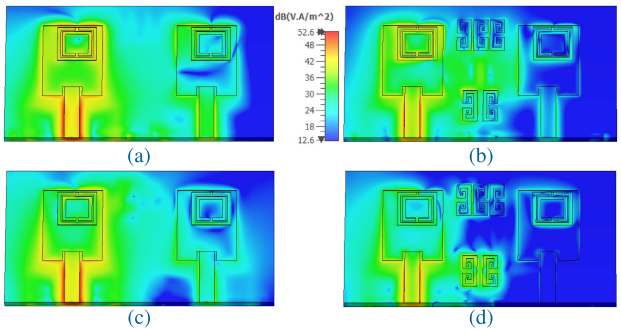

FIGURE 11. Electromagnetic power flow within the structure when port 1 (left) is excited and port 2(right) is connected to 50 Ω: (a) 2.45 GHz without MTMs, (b) 2.45 GHz with MTMs, (c) 5.8 GHz without MTMs, (d) 5.8 GHz with MTMs.

meanders, since feeding port 1 (left antenna) results in only a tiny percentage of the power flowing towards port 2 (right antenna). Regarding the meanders' impact on the antennas, it is observed that they have a negligible effect on their performance and the radiation efficiency is decreased by only 2-5%. This indicates that the meanders re-radiate a high portion of the power that is incident to them rather than dissipating it. Furthermore, in order to avoid the cable effect during the measurements, the ground planes of the antennas are extended in this case as well but only towards one side. The size of the ground extension is carefully chosen through simulations and experiments in order to suppress the cable effect while maintaining the intended performance in terms of S-parameters.

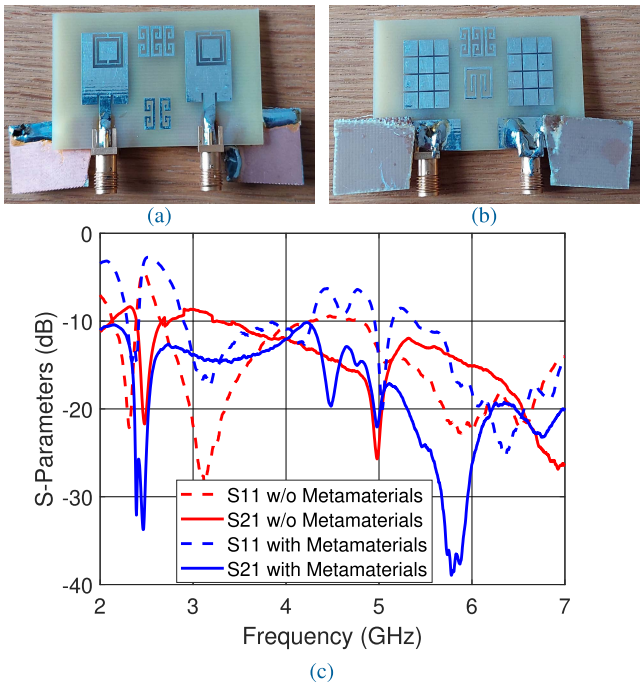

FIGURE 12. Fabricated antennas with the decoupling structure, (a) top view, (b) bottom view, and (c) measured S-parameters (S_{11} and S_{21}) with and without (w/o) metamaterial structures. The ground plane has been extended only towards one side to suppress the cable effect during the measurements.

The fabricated prototype of the two antennas and the measured S-parameters are shown in Fig. 12, while the measured, normalized H-plane radiation patterns of the two antennas at 2.4 and 5.8 GHz are presented in Fig. 13a and Fig. 13b, respectively. Concerning the decoupling performance, the measured isolation levels are increased when metamaterials are utilized while good impedance matching is maintained. Moreover, the radiation patterns are slightly focused towards the left direction for the left antenna and towards the right direction for the right antenna. This is due to the presence of the neighboring antenna's ground plane and the decoupling meanders that reflect and the waves towards these directions. This effect is more intense at the highest frequency band of 5.8 GHz, since the electrical size of the metamaterials and ground plane becomes larger as the frequency increases. In general, an excellent agreement between the simulated and measured radiation patterns is observed.

Furthermore, the simulated 3D radiation patterns of the left antenna (port 1) with and without metamaterial are presented in Figs. 14a-14d. As shown, the metamaterials result in slightly less gain at 2.4 GHz and slightly higher gain at 5.8 GHz. The radiation patterns become more focused towards the left direction due to reflections from the metamaterial cells.

For a fair comparison, Fig. 15 provides the measured realized gains with and without the meanders. Once again, the fabricated prototype operates at 2.37 GHz instead of 2.45 GHz, because the FR-4 has a higher dielectric constant than anticipated. For this reason, the realized gains

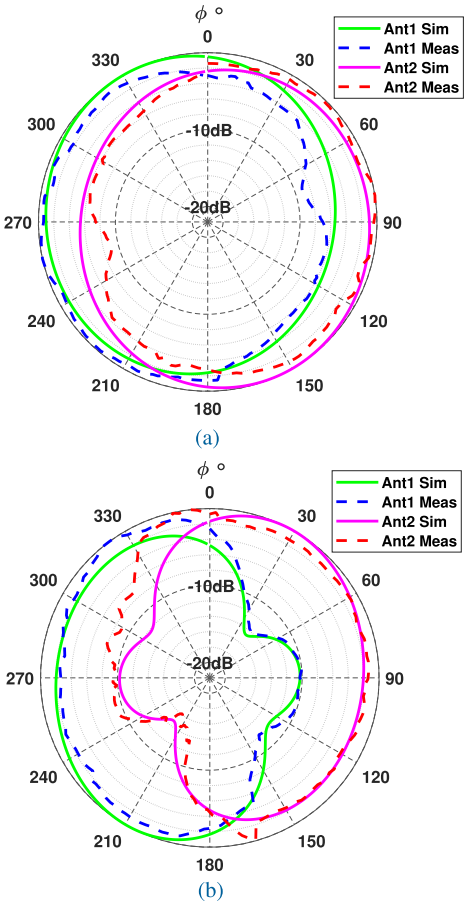

FIGURE 13. Normalized, H-plane, Co-Pol. radiation patterns of the two antennas at (a) 2.4 GHz and (b) 5.8 GHz. Both the simulations and measurements refer to the case with extended ground planes.

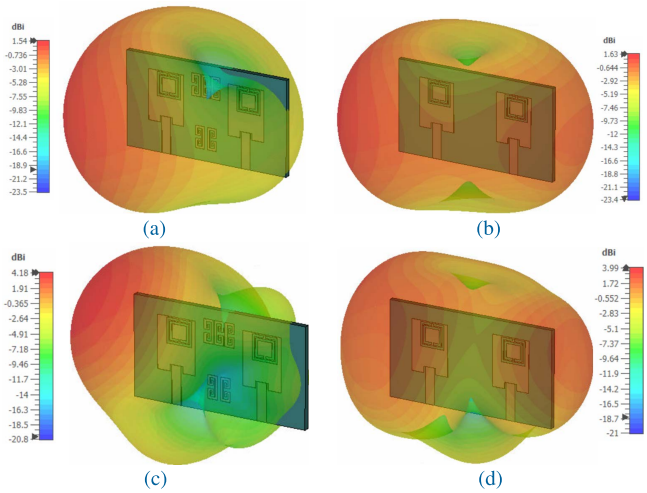

FIGURE 14. 3D radiation patterns of the proposed antennas: (a) 2.4 GHz with MTMs, (b) 2.4 GHz without MTMs, (c) 5.8 GHz with MTMs, (d) 5.8 GHz without MTMs.

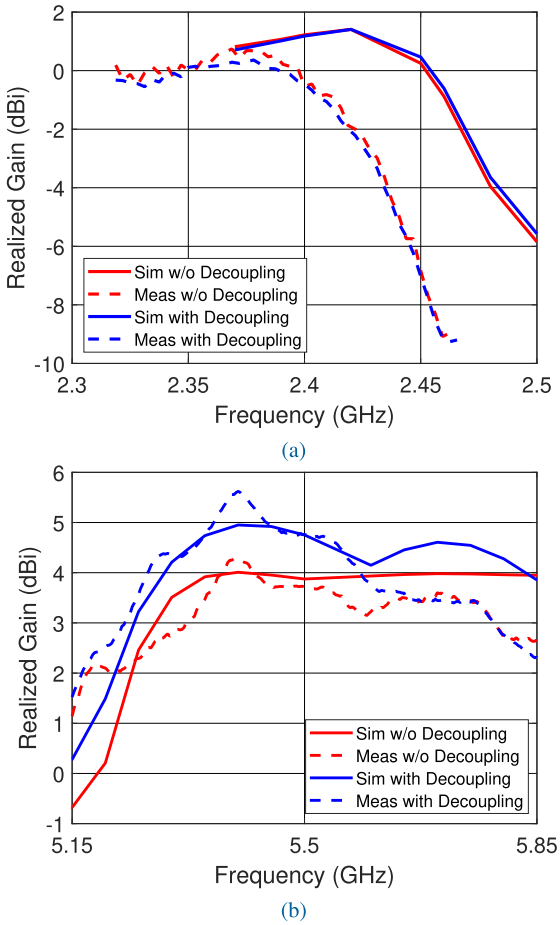

FIGURE 15. Measured realized gain of the proposed antennas with and without metamaterial decoupling at (a) 2.32-2.5 GHz and (b) 5.15-5.85 GHz frequency bands. Both the simulations and measurements refer to the case with extended ground planes. The antenna resonates around 2.37 GHz in practice and therefore the realized gain was measured from 2.32 to 2.45 GHz.

were measured with respect to this new resonance frequency. Despite the fact that the meanders introduce some additional losses, the realized gain at the higher frequency band is improved after the decoupling, while it is only slightly decreased at lower frequencies. More specifically, the realized gain drops from 0.5 to 0 dBi at 2.37 GHz when metamaterials are used. This happens mainly due to the loss associated with the metamaterial meanders that have a small electrical size at the lower band of interest and consequently their ohmic loss is somewhat increased. On the other hand, the metamaterials enhance the gain at the highest frequency band. Here, the gain is improved from 4 to up to 5.5 dBi. This improvement is attributed to the presence of the meanders that have a considerable electrical size at this frequency band and induced currents circulate along their perimeter. Hence, the size of the actual radiating aperture and consequently the gain are increased. Furthermore, less power is absorbed or re-radiated by the adjacent antenna since the isolation levels are improved. Note that due to the extended ground plane the directivity and consequently the realized gain are also increased compared to the initial design. This improvement is about 0.5 - 1 dB.

Another essential figure of merit for multi-antenna systems is the envelope correlation coefficient (ECC). The ECC is calculated by the method reported in [51], which requires the antenna's complex far-field pattern over a sphere. This

TABLE 2. Comparison of the proposed work with previous ones regarding dual-band isolation enhancement.

Reference	[33]	[34]	[35]	[38]	[39]	[41]	Proposed
Decoupling Method	MTM Superstrate	EBG	DGS and Meandering Branch	Decoupling Network	Decoupling and Matching Network	Reactively loaded dummy elements	SNG MTMs
Frequencies (GHz)	2.6 / 3.5	3.48 / 4.88	2.45 / 5.8	1 / 2	2 / 3.7	2.45 / 5.8	2.45 / 5.8
Element Spacing (Edge-to-Edge)	$0.008\lambda_L$/ $0.01\lambda_H$	$0.46\lambda_L$/ $0.65\lambda_H$	$0.12\lambda_L$/ $0.27\lambda_H$	$0.045\lambda_L$/ $0.09\lambda_H$	$0.2\lambda_L$/ $0.37\lambda_H$	$0.13\lambda_L$/ $0.3\lambda_H$	$0.13\lambda_L$/ $0.3\lambda_H$
Antenna Height	$0.1\lambda_L$/ $0.13\lambda_H$	0	0	0	0	0	0
Isolation Enhancement (dB)	26 / 14	26 / 44	12 / 7	33 / 23	24.9 / 20.8	23 / 12	15 / 29
Bandwidth (%)	10 / 11	5 / 8	4 / 10	20 / 10	15 / 3	8 / 5.2	4.1 / 22
Total Efficiency (%)	88 / 67	N/A	75 / 70	70 / 67	89 / 77	65 / 50	60 / 78
Antenna Size	$0.87\lambda_L \times 1.3\lambda_L$	$0.68\lambda_L \times 0.52\lambda_L$	$0.43\lambda_L \times 0.62\lambda_L$	$0.58\lambda_L \times 0.73\lambda_L$	$0.6\lambda_L \times 0.8\lambda_L$	$0.57\lambda_L \times 0.57\lambda_L$	$0.43\lambda_L \times 0.24\lambda_L$

Note: λ_L and λ_H is the free-space wavelength at the lower and higher frequency of the design respectively. The isolation bandwidth is defined as the frequency window where $S_{11} < -10$ dB and the coupling is lower than previously due to the applied isolation technique.

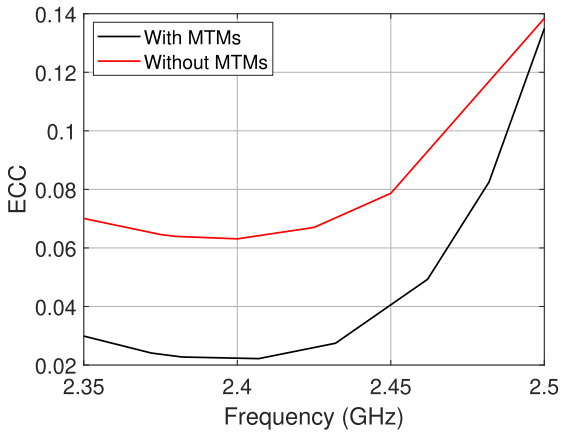

FIGURE 16. Envelope correlation coefficient (ECC) versus frequency at 2.35-2.5 GHz (lower band).

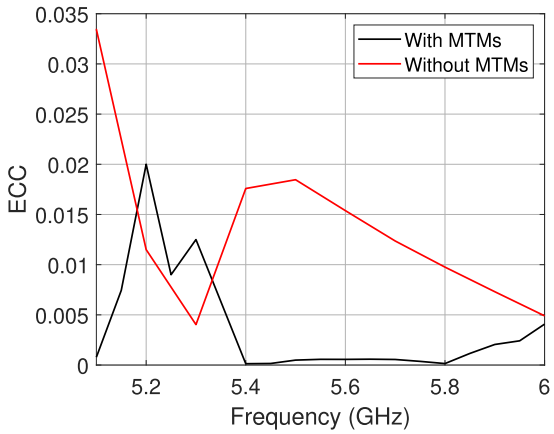

FIGURE 17. Envelope correlation coefficient (ECC) versus frequency at 5-6 GHz (higher band).

method is preferred to the simplified technique based on S-parameters [52], since the latter is less accurate for the lossy antennas that are considered in this paper. The simulated ECC with and without the metamaterial structures are presented in Fig. 16 and Fig. 17 for the lower and higher frequency band, respectively. As shown, it is reduced from 0.08 to 0.04 at 2.45 GHz. Meanwhile, it is always below 0.02 at the higher frequency band of 5-6 GHz.

Finally, table 2 provides a comparison of the proposed antenna with previous works associated with dual-band coupling reduction. Some of the key parameters that are compared are the following: the isolation enhancement due to the applied method, the bandwidth in which the decoupling is achieved, the total efficiency and the total size of the 1×2 antenna system. The proposed antenna design excels

mainly in two categories: i) the isolation bandwidth, where a 22% is accomplished at the higher frequency band, which is the highest among relevant works and ii) the size of the proposed 1×2 antenna, which is the smallest compared to previous designs. This is attributed to the fact that a miniaturized metamaterial antenna is designed as the array's basic unit and thus the overall footprint is considerably reduced. Furthermore, the proposed decoupling techniques do not increase the size of the structure and are seamlessly integrated. This is not the case for prior works that presented superstrates and decoupling networks that increase the overall profile of the structure. Even in the case where the size of the ground plane extension is considered, the combined structure of the antennas and extra ground plane has a total size of $0.56\lambda_L \times 0.29\lambda_L$, which is still smaller than previous reported antennas. On the other hand, it should be mentioned that the compact size of our design comes at the cost of slightly lower total efficiency. The reason for this is that electrically small antennas, such as the ones proposed in this paper, have typically higher loss and lower efficiency compared to normal-sized antennas.

IV. CONCLUSION

The latest trends in wireless communications dictate the use of as small and low-profile devices as possible. In this study, we exploit the metamaterial principles and present an ultra-compact and multi-functional antenna platform. The first contribution of our work is the systematic design of an electrically small antenna loaded with a metaresonator. The proposed antenna covers the commonly used frequency bands of 2.4-2.5/2.9-4.9/5.1-6.5 GHz, while it also exhibits high radiation efficiency and sufficient bandwidth. The second and more important contribution of this work is the decoupling of two of these antennas that have an edge-to-edge separation of only 0.13λ. Contrary to prior art, we provide isolation solutions concerning two frequency bands with minimum impact on the antenna performance and size. By combining the theoretical principles with electromagnetic simulation tools, the design is accelerated and systematic. The isolation improvement from 11 dB to 26 dB at 2.45 GHz and from 16 dB to 45 dB at 5.8 GHz is achieved through the incorporation of meander metamaterials in the structure and it is extremely wideband at higher frequencies. From a theoretical perspective, the proposed antenna platform highlights the benefits of metamaterials in antenna design, where antenna miniaturization and isolation enhancement are usually challenging but necessary tasks. From a practical point of view, it is an ideal candidate for several applications where small size and increased functionality are required.

REFERENCES

[1] L. J. Chu, "Physical limitations of omnidirectional antennas," *J. Appl. Phys.*, vol. 19, pp. 1163–1175, Dec. 1948.
[2] H. A. Wheeler, "Fundamental limitations of small antennas," in *Proc. IRE*, vol. 35, Dec. 1947, pp. 1479–1484.
[3] R. E. Collin and S. Rothschild, "Evaluation of antenna Q," *IEEE Trans. Antennas Propag.*, vol. AP-12, no. 1, pp. 23–27, Jan. 1964.
[4] J. S. McLean, "A re-examination of the fundamental limits on the radiation Q of electrically small antennas," *IEEE Trans. Antennas Propag.*, vol. 44, no. 5, pp. 672–676, May 1996.
[5] C. Milias, R. B. Andersen, P. I. Lazaridis, Z. D. Zaharis, B. Muhammad, J. T. B. Kristensen, A. Mihovska, and D. D. S. Hermansen, "Metamaterial-inspired antennas: A review of the state of the art and future design challenges," *IEEE Access*, vol. 9, pp. 89846–89865, 2021.
[6] T. Kokkinos and A. P. Feresidis, "Electrically small superdirective endfire arrays of metamaterial-inspired low-profile monopoles," *IEEE Antennas Wireless Propag. Lett.*, vol. 11, pp. 568–571, 2012.
[7] T. Kokkinos and A. P. Feresidis, "Low-profile folded monopoles with embedded planar metamaterial phase-shifting lines," *IEEE Trans. Antennas Propag.*, vol. 57, no. 10, pp. 2997–3008, Oct. 2009.
[8] K. Konstantinidis, A. P. Feresidis, and P. S. Hall, "Broadband subwavelength profile high-gain antennas based on multi-layer metasurfaces," *IEEE Trans. Antennas Propag.*, vol. 63, no. 1, pp. 423–427, Jan. 2015.
[9] T. Negishi, D. Erricolo, and P. L. E. Uslenghi, "Metamaterial spheroidal cavity to enhance dipole radiation," *IEEE Trans. Antennas Propag.*, vol. 63, no. 6, pp. 2802–2807, Jun. 2015.
[10] G. Oliveri, D. H. Werner, and A. Massa, "Reconfigurable electromagnetics through metamaterials—A review," *Proc. IEEE*, vol. 103, no. 7, pp. 1034–1056, Jul. 2015.
[11] M. A. Antoniades and G. V. Eleftheriades, "Compact linear lead/lag metamaterial phase shifters for broadband applications," *IEEE Antennas Wireless Propag. Lett.*, vol. 2, pp. 103–106, 2003.
[12] O. Isik and K. P. Esselle, "Backward wave microstrip lines with complementary spiral resonators," *IEEE Trans. Antennas Propag.*, vol. 56, no. 10, pp. 3173–3178, Oct. 2008.
[13] G. Oliveri, E. T. Bekele, M. Salucci, and A. Massa, "Array miniaturization through QCTO-SI metamaterial radomes," *IEEE Trans. Antennas Propag.*, vol. 63, no. 8, pp. 3465–3476, Aug. 2015.
[14] G. Oliveri, E. T. Bekele, M. Salucci, and A. Massa, "Transformation electromagnetics miniaturization of sectoral and conical metamaterial-enhanced horn antennas," *IEEE Trans. Antennas Propag.*, vol. 64, no. 4, pp. 1508–1513, Apr. 2016.
[15] M. A. Antoniades, J. Zhu, M. Seivanayagam, and G. V. Eleftheriades, "Compact, wideband and multiband antennas based on metamaterials concepts," in *Proc. 4th Europ. Conf. Antennas Prop. (EuCAP)*, Barcelona, Spain, Apr. 2010, pp. 1–5.
[16] M. Kovaleva, D. Bulger, and K. P. Esselle, "Cross-entropy method for design and optimization of pixelated metasurfaces," *IEEE Access*, vol. 8, pp. 224922–224931, 2020.
[17] Y. Ge, K. P. Esselle, and T. S. Bird, "The use of simple thin partially reflective surfaces with positive reflection phase gradients to design wideband, low-profile EBG resonator antennas," *IEEE Trans. Antennas Propag.*, vol. 60, no. 2, pp. 743–750, Feb. 2012.
[18] R. W. Ziolkowski and A. Erentok, "Metamaterial-based efficient electrically small antennas," *IEEE Trans. Antennas Propag.*, vol. 54, no. 7, pp. 2113–2130, Jul. 2006.
[19] D. K. Ntaikos, N. K. Bourgis, and T. V. Yioultsis, "Metamaterial-based electrically small multiband planar monopole antennas," *IEEE Antennas Wireless Propag. Lett.*, vol. 10, pp. 963–966, 2011.
[20] K. Li, C. Zhu, L. Li, Y.-M. Cai, and C.-H. Liang, "Design of electrically small metamaterial antenna with ELC and EBG loading," *IEEE Antennas Wireless Propag. Lett.*, vol. 12, pp. 678–681, 2013.
[21] J. Zhu and G. V. Eleftheriades, "Dual-band metamaterial-inspired small monopole antenna for WiFi applications," *Electron. Lett.*, vol. 45, no. 22, pp. 1104–1106, Oct. 2009.
[22] J. Zhu, M. A. Antoniades, and G. V. Eleftheriades, "A compact tri-band monopole antenna with single-cell metamaterial loading," *IEEE Trans. Antennas Propag.*, vol. 58, no. 4, pp. 1031–1038, Apr. 2010.
[23] X. Chen, S. Zhang, and Q. Li, "A review of mutual coupling in MIMO systems," *IEEE Access*, vol. 6, pp. 24706–24719, 2018.
[24] E. G. Larsson, O. Edfors, F. Tufvesson, and T. L. Marzetta, "Massive MIMO for next generation wireless systems," *IEEE Commun. Mag.*, vol. 52, no. 2, pp. 186–195, Feb. 2014.
[25] P. N. Fletcher, M. Dean, and A. R. Nix, "Mutual coupling in multi-element array antennas and its influence on MIMO channel capacity," *Electron. Lett.*, vol. 39, no. 4, p. 342, 2003.
[26] J. Diao and K. F. Warnick, "Antenna loss and receiving efficiency for mutually coupled arrays," *IEEE Trans. Antennas Propag.*, vol. 65, no. 11, pp. 5871–5877, Nov. 2017.

[27] X. Chen, M. Abdullah, Q. Li, J. Li, A. Zhang, and T. Svensson, "Characterizations of mutual coupling effects on switch-based phased array antennas for 5G millimeter-wave mobile communications," *IEEE Access*, vol. 7, pp. 31376–31384, 2019.
[28] A. Alu, N. Engheta, A. Erentok, and R. W. Ziolkowski, "Single-negative, double-negative, and low-index metamaterials and their electromagnetic applications," *IEEE Antennas Propag. Mag.*, vol. 49, no. 1, pp. 23–36, Feb. 2007.
[29] D. A. Ketzaki and T. V. Yioultsis, "Metamaterial-based design of planar compact MIMO monopoles," *IEEE Trans. Antennas Propag.*, vol. 61, no. 5, pp. 2758–2766, Jan. 2013.
[30] M. G. Alsath, M. Kanagasabai, and B. Balasubramanian, "Implementation of slotted meander-line resonators for isolation enhancement in microstrip patch antenna arrays," *IEEE Antennas Wireless Propag. Lett.*, vol. 12, pp. 15–18, 2013.
[31] S. R. Thummaluru and R. K. Chaudhary, "Mu-negative metamaterial filter-based isolation technique for MIMO antennas," *Electron. Lett.*, vol. 53, no. 10, pp. 644–646, 2017.
[32] M. M. Bait-Suwailam, M. S. Boybay, and O. M. Ramahi, "Electromagnetic coupling reduction in high-profile monopole antennas using single-negative magnetic metamaterials for MIMO applications," *IEEE Trans. Antennas Propag.*, vol. 58, no. 9, pp. 2894–2902, Sep. 2010.
[33] F. Liu, J. Guo, L. Zhao, G.-L. Huang, Y. Li, and Y. Yin, "Dual-band metasurface-based decoupling method for two closely packed Dual-band antennas," *IEEE Trans. Antennas Propag.*, vol. 68, no. 1, pp. 552–557, Jan. 2020.
[34] X. Tan, W. Wang, Y. Wu, Y. Liu, and A. A. Kishk, "Enhancing isolation in dual-band meander-line multiple antenna by employing split EBG structure," *IEEE Trans. Antennas Propag.*, vol. 67, no. 4, pp. 2769–2774, Apr. 2019.
[35] J. Y. Deng, J. Li, L. Zhao, and L. Guo, "A dual-band inverted-F MIMO antenna with enhanced isolation for WLAN applications," *IEEE Antennas Wireless Propag. Lett.*, vol. 16, pp. 2270–2273, 2017.
[36] Z. Ren and A. Zhao, "Dual-band MIMO antenna with compact self-decoupled antenna pairs for 5G mobile applications," *IEEE Access*, vol. 7, pp. 82288–82296, 2019.
[37] W. Wang, Y. Wu, W. Wang, and Y. Yang, "Isolation enhancement in dual-band monopole antenna for 5G applications," *IEEE Trans. Circuits Syst. II, Exp. Briefs*, vol. 68, no. 6, pp. 1867–1871, Jun. 2021.
[38] M. Li, J. M. Yasir, K. L. Yeung, and L. Jiang, "A novel dual-band decoupling technique," *IEEE Trans. Antennas Propag.*, vol. 68, no. 10, pp. 6923–6934, Oct. 2020.
[39] K.-D. Xu, H. Luyen, and N. Behdad, "A decoupling and matching network design for single- and dual-band two-element antenna arrays," *IEEE Trans. Microw. Theory Techn.*, vol. 68, no. 9, pp. 3986–3999, Sep. 2020.
[40] M. Li, Y. Zhang, D. Wu, K. L. Yeung, L. Jiang, and R. Murch, "Decoupling and matching network for dual-band MIMO antennas," *IEEE Trans. Antennas Propag.*, vol. 70, no. 3, pp. 1764–1775, Mar. 2022.
[41] X. Shen, F. Liu, L. Zhao, G.-L. Huang, X. Shi, Q. Huang, and A. Chen, "Decoupling of two strongly coupled dual-band antennas with reactively loaded dummy element array," *IEEE Access*, vol. 7, pp. 154672–154682, 2019.
[42] Y. Dong, H. Toyao, and T. Itoh, "Design and characterization of miniaturized patch antennas loaded with complementary split-ring resonators," *IEEE Trans. Antennas Propag.*, vol. 60, no. 2, pp. 772–785, Feb. 2012.
[43] *CST Microwave Studio*. Accessed: Dec. 2021. [Online]. Available: http://www.cst.com
[44] A. D. Yaghjian and S. R. Best, "Impedance, bandwidth, and Q of antennas," *IEEE Trans. Antennas Propag.*, vol. 53, no. 4, pp. 1298–1324, Apr. 2005.
[45] T. Fukasawa, N. Yoneda, and H. Miyashita, "Investigation on current reduction effects of baluns for measurement of a small antenna," *IEEE Trans. Antennas Propag.*, vol. 67, no. 7, pp. 4323–4329, Jul. 2019.
[46] Z. N. Chen, N. Yang, Y.-X. Guo, and M. Y. W. Chia, "An investigation into measurement of handset antennas," *IEEE Trans. Instrum. Meas.*, vol. 54, no. 3, pp. 1100–1110, Jun. 2005.
[47] Y. M. Pan, K. W. Leung, and K. Lu, "Compact quasi-isotropic dielectric resonator antenna with small ground plane," *IEEE Trans. Antennas Propag.*, vol. 62, no. 2, pp. 577–585, Feb. 2014.
[48] L. Huitema, C. Delaveaud, and R. D'Errico, "Impedance and radiation measurement methodology for ultra miniature antennas," *IEEE Trans. Antennas Propag.*, vol. 62, no. 7, pp. 3463–3473, Jul. 2014.
[49] A. B. Numan and M. S. Sharawi, "Extraction of material parameters for metamaterials using a full-wave simulator [education column]," *IEEE Antennas Propag. Mag.*, vol. 55, no. 5, pp. 202–211, Oct. 2013.
[50] D. R. Smith, D. C. Vier, T. Koschny, and C. M. Soukoulis, "Electromagnetic parameter retrieval from inhomogeneous metamaterials," *Phys. Rev. E, Stat. Phys. Plasmas Fluids Relat. Interdiscip. Top.*, vol. 71, no. 3, Mar. 2005, 036617.
[51] R. G. Vaughan and J. B. Andersen, "Antenna diversity in mobile communications," *IEEE Trans. Veh. Technol.*, vol. VT-36, no. 4, pp. 149–172, Nov. 1987.
[52] S. Blanch, J. Romeu, and I. Corbella, "Exact representation of antenna system diversity performance from input parameter description," *Electron. Lett.*, vol. 39, no. 9, pp. 705–707, May 2003.

CHRISTOS MILIAS (Student Member, IEEE) was born in Drama, Greece, in 1997. He received the M.Sc. degree in electrical and computer engineering from the Aristotle University of Thessaloniki, Thessaloniki, Greece, in 2020. He is currently pursuing the dual Ph.D. degree with MyDefence ApS, Nørresundby, Denmark, and the Department of Business and Technology (BTECH), Aarhus University, Denmark. His research interests include antennas and propagation, metamaterials, and radar systems.

RASMUS B. ANDERSEN received the M.S. degree in advanced radio frequency design from Aalborg University, Denmark, in 2001. He has been working in the telecommunication industry, since 2001, implementing RF systems from antenna to software defined baseband. From 2011 to 2016, he worked as a Project Manager within organic photovoltaics at Mekoprint and joined MyDefence, in 2016, as a Senior Hardware Engineer with focus on drone RF sensors, electronic counter measures, and radar sensing. He has headed projects in the fields of product development, commercial-academic collaboration, MIL-STD and medical approvals, process control, and application engineering.

PAVLOS I. LAZARIDIS (Senior Member, IEEE) received the M.Eng. degree in electrical engineering from the Aristotle University of Thessaloniki, Greece, in 1990, the M.Sc. degree in electronics from Université Pierre and Marie Curie (Paris 6), Paris, France, in 1992, and the dual Ph.D. degree from the École Nationale Supérieure des Télécommunications (ENST), Paris, and Université Paris 6, in 1996. From 1991 to 1996, he was involved with research for France Télécom, and teaching at ENST Paris. In 1997, he became the Head of the Antennas and Propagation Laboratory, Télédiffusion de France/France Télécom Research Center (TDF-C2R Metz). From 1998 to 2002, he was a Senior Examiner at the European Patent Office (EPO), The Hague, The Netherlands. From 2002 to 2014, he was involved with teaching and research with the ATEI of Thessaloniki, Greece, and Brunel University, London, U.K. He is currently a Professor in electronics and telecommunications with the University of Huddersfield, U.K. He has been involved in several international research projects, such as EU Horizon 2020 MOTOR5G and RECOMBINE, NATO-SfP ORCA. He has published over 150 research papers and several national and European patents. He is a member of the IET (MIET), a Senior Member of URSI, and a fellow of the Higher Education Academy (FHEA). He is currently serving as an Associate Editor for IEEE Access.

ZAHARIAS D. ZAHARIS (Senior Member, IEEE) received the B.Sc. degree in physics, the M.Sc. degree in electronics, the Ph.D. degree in antennas and propagation modeling for mobile communications, and the Diploma degree in electrical and computer engineering from the Aristotle University of Thessaloniki, Thessaloniki, Greece, in 1987, 1994, 2000, and 2011, respectively. From 2002 to 2013, he was with the Administration of the Telecommunications Network, Aristotle University of Thessaloniki, where he has been with the Department of Electrical and Computer Engineering, since 2013. His current research interests include design and optimization of antennas and microwave circuits, signal processing on smart antennas, development of evolutionary optimization algorithms, and neural networks. He is a member of the Technical Chamber of Greece. He is currently serving as an Associate Editor for IEEE Access.

BILAL MUHAMMAD received the Ph.D. degree in telecommunication engineering from the University of Rome Tor Vergata, Italy. He is currently working as an Assistant Professor with the Department of Business Development and Technology (BTECH), Aarhus University, Denmark. His research interests include UAV wireless communication for 5G and beyond, GNSS integrity and accuracy for UAV, unmanned traffic management (UTM) systems and services, multi-business model innovation, and prototyping UAV applications. He actively participates in EU projects and has been the WP Leader for SARA and EASY-PV projects funded under H2020 Innovation Action Program.

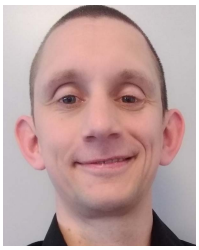

JES T. B. KRISTENSEN received the M.Sc. degree in electrical engineering from Aalborg University, Denmark, in 2008, with a specialization in applied signal processing and implementation. From 2008 to 2014, he worked at Rohde & Schwarz (TCDK—Aalborg/Denmark and Munich) as an FPGA and a Baseband Developer for WCDMA L1 testing for the CRTU and CMW500 products. Additionally, he worked as a Technical Consultant for starting and facilitating the TD-SCDMA development with R&S China and the Beijing universities. Since 2014, he has been working at MyDefence (http://mydefence.dk), Denmark, as a Signal Processing Engineer and a General Architect for C-UAV sensors. Defining the core of the RF-sensors and radars in the company portfolio—the Wingman-, Watchdog-, Wolfpack-, and Eagle-products among others. In addition, he serves as a SCRUM Master, a Process Enthusiast and as an Ad-Hoc Technical Project Lead for i.e., tenders, research, product development and the EU KNOX Horizon 2020 project. For more information visit the link (https://www.linkedin.com/in/jestoftkristensen/).

ALBENA MIHOVSKA (Member, IEEE) received the Ph.D. degree in mobile communications from Aalborg University, Denmark. She has been an Associate Professor with the Department of Business Development and Technology, Aarhus University, Denmark, since 2017, where she is leading the research activities of the 6G Knowledge Laboratory with a focus on 6G connectivity and enabling technologies (e.g., artificial intelligence) and advanced services and applications, such as augmented and extended reality (AR, XR), high-fidelity and real time mobile hologram, and digital twins. She is also a Senior Research and an Academic Professional. She has more than 150 scientific publications.

DAN D. S. HERMANSEN received the M.Sc. degree in RF engineering and CMOS IC design from Aalborg University, Denmark, in 2005. He has worked in the telecommunication industry for over 20 years on RF related systems and technologies. In 2013, he co-founded MyDefence, which works with security related applications like anti-drone equipment, including RF sensors, RF jammers, radars, and data fusion. MyDefence has completed numerous research projects within the EU (e.g., H2020), Danish Defence, and Innovation Fund Denmark Research Program, where he has headed the projects.